Robotics and Computer–Integrated Manufacturing 79 (2023) 102446

Contents lists available at ScienceDirect

Robotics and Computer-Integrated Manufacturing

journal homepage: www.elsevier.com/locate/rcim

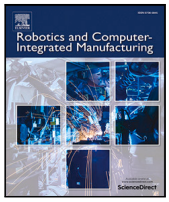

Full length article

Kinematic calibration for collaborative robots on a mobile platform using motion capture system

Leon Žlajpah, Tadej Petrič *

Jožef Stefan Institute, Jamova c. 39, Ljubljana, 1000, Slovenia

ARTICLE INFO

Keywords:
Serial robot manipulators
Kinematic parameter identification
Optical tracking system

ABSTRACT

For modern robotic applications that go beyond the typical industrial environment, absolute accuracy is one of the key properties that make this possible. There are several approaches in the literature to improve robot accuracy for a typical industrial robot mounted on a fixed frame. In contrast, there is no method to improve robot accuracy when the robot is mounted on a mobile base, which is typical for collaborative robots. Therefore, in this work, we proposed and analyzed two approaches to improve the absolute accuracy of the robot mounted on a mobile platform using an optical measurement system. The first approach is based on geometric operations used to calculate the rotation axes of each joint. This approach identifies all rotational axes, which allows the calculation of the Denavit–Hartenberg (DH) parameters and thus the complete kinematic model, including the position and orientation errors of the robot end-effector and the robot base. The second approach to parameter estimation is based on optimization using a set of joint positions and end-effector poses to find the optimal DH parameters. Since the robot is mounted on a mobile base that is not fixed, an optical measurement system was used to dynamically and simultaneously measure the position of the robot base and the end-effector. The performance of the two proposed methods was analyzed and validated on a 7-DoF Franka Emika Panda robot mounted on a mobile platform PAL Tiago-base. The results show a significant improvement in absolute accuracy for both proposed approaches. By using the proposed approach with the optical measurement system, we can easily automate the estimation of robot kinematic parameters with the aim of improving absolute accuracy, especially in applications that require high positioning accuracy.

1. Introduction

Nowadays, robots are widely used in industry to automate manufacturing processes in order to increase efficiency and production. For high-volume production processes, a typical programming strategy is to move the robot to the desired position, which is recorded and then repeated. In contrast, such programming would not be economically viable for low-volume production, as it is usually very time-consuming. On the other hand, offline programming strategies could be used to bridge the gap, but they require absolute robot accuracy to perform the task on a real robot. In this case, knowledge of robot kinematics is essential. Usually, robot manufacturers provide a nominal kinematic model of the robots in the form of Denavit–Hartenberg (DH) parameters, which differs from the actual model due to errors in robot manufacturing, assembly, etc. Often the nominal parameters are also not generally accessible because they are used internally by the robot controller. All of this limits the practical use of robots in many low-volume applications.

To reduce the kinematic error between robots and thus enable wider practical use, several online and offline methods have been described in the literature, all aimed at improving the absolute accuracy of the robot [1,2]. In general, we can divide kinematic calibration into two groups based on the measurement method used. The open-loop method, where the absolute position of the robot is measured, and the closed-loop method, where the position of the robot is measured relative to the reference frame. In general, however, both methods require a reference measuring system to determine the kinematic parameters. Systems such as, laser trackers [3,4], conventional or optical coordinate measuring machines [5], ball bars [6], etc. can be used. The most typical of them are listed in Table 1, where we compare their strengths and weaknesses. Note that there are also generally no prescribed guidelines or procedures to determine the quality of kinematic identification with any of the measurement systems. Usually, open-loop calibration of DH parameters with a laser tracker leads to higher accuracy, but it

* Corresponding author.
Tadej Petrič, Linkedin: tadej-petric-298b35166 (T. Petrič).
E-mail addresses: leon.zlajpah@ijs.si (L. Žlajpah), tadej.petric@ijs.si (T. Petrič).
URLs: https://abr.ijs.si/people/leon-zlajpah/ (L. Žlajpah), http://cobotat.ijs.si/members/tadej-petric/ (T. Petrič).

https://doi.org/10.1016/j.rcim.2022.102446
Received 13 April 2022; Received in revised form 24 June 2022; Accepted 16 August 2022
Available online 1 September 2022

Table 1
Comparison of different measurement systems for kinematic identification.
Source: Adapted from [11].

Devices | Features	Repeatability	MC	Port.	EoU	Cost	MoB	6DP
Theodolite	5–10 mm	Static	High	Low	Medium	No	Static
Ultrasonic trilateration	1 mm	Dynamic	High	Medium	Low	No	Static
Machine vision	0.8–1 mm	Dynamic	High	Medium	Medium	Yes	Dynamic
Laser tracker	10 μm	Dynamic	High	Medium	High	No	Static
IR Motion Capture System	0.1 mm	Dynamic	Medium	Medium	Medium	Yes	Dynamic

MC: Measurement Characteristic, Port.: Portability, EoU: Ease of use, MoB: Mobile Base, 6DP: 6D DoF pose (position and orientation).

is costly and not flexible [7,8]. The cheapest alternative is to use a close-loop approach with precise measurement devices, but it requires manual robot guidance. Consequently, such an approach is difficult to automate, which affects the overall accuracy of the calibration [9,10]. The literature, procedures and measurement systems for kinematic calibration of robots on mobile platforms are even sparser. As can be seen from Table 1, only machine vision systems or motion capture systems can be used when the robot is attached to a mobile base since only these systems can simultaneously measure the positions of the end-effector and the robot base. Due to increasing number of collaborative robots, better accessibility and their introduction into new areas ranging from production lines to our everyday environment, improving absolute accuracy is still a challenge for robotics.

Recent research on kinematic calibration includes the iterative optimization process based on least-square theory for the typical 6-DoF industrial robots [12]. An automatic algorithm for identifying DH parameters of serial manipulators was also proposed in [13], where a geometric operation and dual vector algebra were used to determine the relative transformation matrices from which the DH parameters are then calculated. In [14], they reported on the combination of geometric and parametric identification methods to take advantage of both methods for industrial robots. They showed that their method works well even when the workspace is constrained. Similarly, in [11], a general formulation for identifying the kinematic parameters of an industrial robot using a geometric approach was proposed when no prior information about the robot kinematics is available. They used a monocular camera to identify the parameters of a typical 6 DOF industrial robot. In [9], an indexed measurement platform was used as a measurement platform to identify kinematic parameters. The evaluation of accuracy in the calibration of kinematic parameters of industrial robots was analyzed in [15], with the aim of improving on-site calibration. Similarly, but with a rigid–flexible coupling error model consisting of geometric and compliance errors for industrial robots with non-negligible flexibility was used in [16]. In addition to typical industrial robots, parameter identification and calibration of a non-fully symmetric parallel delta robot was reported in [7]. In most of these approaches, it is not possible to measure the base and the end-effector at the same time, which is also evident from Table 1. This would otherwise be possible with an optical measurement system or a motion capture system. The literature here is sparse, in [17] they have integrated a numerical least squares algorithm for identifying kinematic parameters. However, none of these methods address kinematic parameter identification for collaborative robots, which typically have 7 DOF and are mounted on a mobile base.

To address this gap, we propose a kinematic calibration approach for mobile collaborative robots. Although kinematic calibration is a well researched field, most of the proposed methods require a fixed and stationary base to perform measurements with external measurement instruments, such as laser trackers or some kind of mechanical devices. In contrast, the base of a mobile robot is never completely fixed. Even if the base is stationary, the movement of the robot can cause some movements of the base. Therefore, our goal was to calibrate the robot attached to the mobile base, which requires measuring the positions of the base and the end-effector simultaneously. Therefore, in this work, we propose to use a optical motion tracking system similar to [17], except that our system uses passive markers. Based on the measurements, we analyzed and compared two approaches for the identification of DH parameters: one based on geometric operations as in [13], but with an extension that takes into account the mobile base, and a second in which the DH parameters are identified using optimization.

While many proposed approaches address the calibration problem by introducing corrections in the final end-effector pose, our approach focuses on correcting the kinematic model of the robot, i.e. DH parameters. Accurate models are essential for human–robot and most robot–robot collaborations, where the interaction between robots depends heavily on the underlying method. The contribution of this work, going beyond our preliminary report [18], may be summarized as follows: (i) a geometric and numerical approach for the calibration of collaborative robots mounted on a mobile base; (ii) analysis of the influence of the accuracy of the motion tracking system on the accuracy of DH parameter estimation; (iii) experimental evaluation of different methods for DH parameter estimation.

The paper is organized as follows. In Section 2, we give an overview of kinematic modeling of a robot and in Section 3 we give algorithms for identification of DH parameters. In Section 4, we describe our experimental setup and measurement procedures. In Section 5 we provide results and compare different calibration strategies. Conclusions can be found in Section 6.

2. Kinematic model parameters

A serial robot manipulator consists of links connected by joints. The joints can be of different types and have one or more degrees of freedom (DOF). However, since most modern robots use only rotary joints, we assume in the following that the robot has only rotary joints with one DOF.

For the kinematic analysis, we add a coordinate frame to each link. In particular, the frame $\mathcal{F}_i$ with origin $\boldsymbol{p}_i$ and orientation axes $(\boldsymbol{x}_i, \boldsymbol{y}_i, \boldsymbol{z}_i)$ is connected to the link i and the joint i connects the frames $\mathcal{F}_{i-1}$ and $\mathcal{F}_i$. Note that $\mathcal{F}_0$ represents the base frame of the robot and $\mathcal{F}_n$ is connected to the end-effector of the robot. The transformation between the frames $\mathcal{F}_{i-1}$ and $\mathcal{F}_i$ is expressed by the homogeneous transformation matrix ${}^{i-1}\mathbf{T}_i(q_i)$, where q_i is a common variable (position). Thus, the transformation between the robot base and the end-effector is given as

$$ {}^0\mathbf{T}_E(\boldsymbol{q}) = \begin{bmatrix} \mathbf{R}_E & \boldsymbol{p}_E \\ \mathbf{0} & 1 \end{bmatrix} = {}^0\mathbf{T}_n(\boldsymbol{q}) {}^n\mathbf{T}_E = \left(\prod_{i=1}^{n} {}^{i-1}\mathbf{T}_i(q_i) \right) {}^n\mathbf{T}_E \,, \tag{1} $$

where ${}^n\mathbf{T}_E$ is a fixed transformation matrix between the robot flange and the end-effector frame $\mathcal{F}_E$. Since the end-effector pose is the position and orientation of the end-effector frame $\mathcal{F}_E$, (1) represents the forward kinematics mapping the joint variables $\boldsymbol{q}$ to the end-effector pose and can also be written in the form

$$ f(\boldsymbol{q}) = \{ \boldsymbol{p}_E(\boldsymbol{q}), \mathcal{Q}_E(\boldsymbol{q}) \} \tag{2} $$

where $\boldsymbol{p}$ is the position of the end-effector and $\mathcal{Q}$ is a quaternion representing the orientation of the end-effector $\mathbf{R}$.

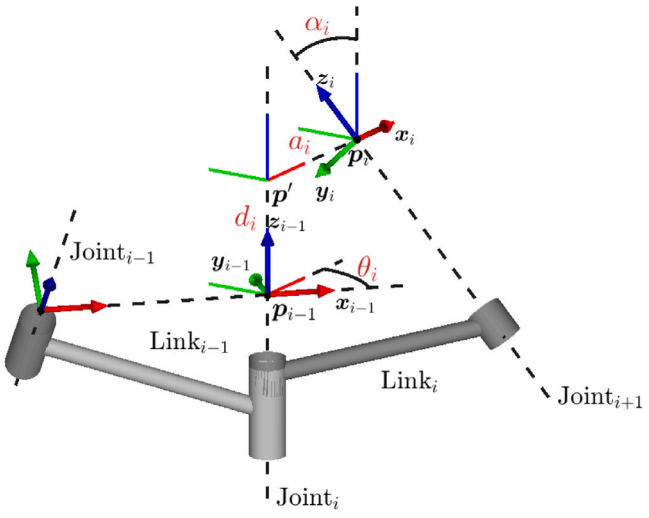

Fig. 1. DH parameters for serial robot manipulators.

2.1. Denavit–Hartenberg parameters

Various models have been proposed to calculate the direct kinematic Eq. (1). However, the most commonly used approach is the Denavit–Hartenberg (DH) convention [19], which provides a minimal representation and an intuitive method for determining its parameters using linear algebra.

According to the DH convention, the z-axes of the frames $\mathcal{F}_i$ are aligned with the corresponding joints and the x-axes are parallel to the common normal of the successive joint axes, as shown in Fig. 1. Then, a set of four parameters a, α, d and θ is used to define the transformation ${}^{i-1}\mathbf{T}_i$

$$ {}^{i-1}\mathbf{T}_i(q_i) = \mathrm{Rot}_{\boldsymbol{z}_{i-1}}(\theta_i) \cdot \mathrm{Trans}_{\boldsymbol{z}_{i-1}}(d_i) \cdot \mathrm{Trans}_{\boldsymbol{x}_i}(a_i) \cdot \mathrm{Rot}_{\boldsymbol{x}_i}(\alpha_i)\,, \tag{3} $$

where $\mathrm{Trans}_{\boldsymbol{a}}(\cdot)$ and $\mathrm{Rot}_{\boldsymbol{a}}(\cdot)$ represent the translation and rotation along vector $\boldsymbol{a}$, respectively. The transformation matrix ${}^{i-1}\mathbf{T}_i$ is a function of the joint variable q_i and for a revolute joint q_i corresponds to θ. So, θ_i is actually the offset of the joint variable q_i. From (3) we therefore obtain

$$ {}^{i-1}\mathbf{T}_i(q_i) = \begin{bmatrix} \cos(\hat{q}_i) & -\cos(\alpha_i)\sin(\hat{q}_i) & \sin(\alpha_i)\sin(\hat{q}_i) & a_i\cos(\hat{q}_i) \\ \sin(\hat{q}_i) & \cos(\alpha_i)\cos(\hat{q}_i) & -\sin(\alpha_i)\cos(\hat{q}_i) & a_i\sin(\hat{q}_i) \\ 0 & \sin(\alpha_i) & \cos(\alpha_i) & d_i \\ 0 & 0 & 0 & 1 \end{bmatrix}, \tag{4} $$

where

$$ \hat{q}_i = q_i + \theta_i\,. \tag{5} $$

3. Identification of DH parameters

The manufacturer of a robot usually provides the nominal values of the DH parameters or some other data that can be used to calculate the DH parameters. However, the actual DH parameters of a robot may differ from the nominal values due to manufacturing or assembly errors. Therefore, to reduce the positioning errors of the end-effector, it is necessary to identify the actual kinematic parameters of a robot, in our case the exact DH parameters.

3.1. Geometric approach

A straightforward method for calculating DH parameters is a geometric approach based on known joint axes and linear algebra. Assuming that the joint axes $\boldsymbol{z}_i, i = 1,\dots,n$ are known, the parameters can be determined in two steps: determining the relative frames for each joint and computing the DH parameters using these two frames. The procedure is recursive, starting from the base of the robot and moving towards the end-effector. The pose (position and orientation) of the frame $\mathcal{F}_i$ is determined by the intersection or the nearest points of the lines defined by the joint axes $\boldsymbol{z}_{i-1}$ and $\boldsymbol{z}_i$.

Knowing the frame $\mathcal{F}_{i-1}$ and the line on which the axis of the next joint ($\boldsymbol{z}_i$) lies, we first calculate the intersections or nearest points of the lines defined by $\boldsymbol{z}_{i-1}$ and $\boldsymbol{z}_i$. Then the pose of the frame $\mathcal{F}_i$ is determined in the following way (see also Fig. 1):

1. Per definition, $\boldsymbol{z}_{i-1}$ represents the axis of the ith joint.
2. The frame origins $\boldsymbol{p}'$ and $\boldsymbol{p}_i$ are located at the closest points on the lines defined by $\boldsymbol{z}_{i-1}$ and $\boldsymbol{z}_i$, respectively.
3. Axis $\boldsymbol{x}_i$ can be determined from the common normal to both joint axes, i.e., it is in the direction from $\boldsymbol{p}'$ to $\boldsymbol{p}_i$.
4. Axis $\boldsymbol{y}_i$ is directly determined once the $\boldsymbol{z}_i$ and $\boldsymbol{x}_i$ are known, $\boldsymbol{y}_i = \boldsymbol{z}_i \times \boldsymbol{x}_i$.

After calculating the coordinate frames $\mathcal{F}_{i-1}$ and $\mathcal{F}_i$, the DH parameters used to describe each transformation ${}^{i-1}\mathbf{T}_i$ are calculated as follows:

- angle θ_i between x-axes $\boldsymbol{x}_{i-1}$ and $\boldsymbol{x}_i$ around z-axis $\boldsymbol{z}_{i-1}$

$$ \theta_i = \mathrm{atan2}\left((\boldsymbol{x}_{i-1} \times \boldsymbol{x}_i) \cdot \boldsymbol{z}_{i-1}, \boldsymbol{x}_{i-1} \cdot \boldsymbol{x}_i\right) \tag{6} $$

- distance d_i between the origins $\boldsymbol{p}_{i-1}$ to $\boldsymbol{p}'$ (to the common normal)

$$ d_i = (\boldsymbol{p}_i - \boldsymbol{p}_{i-1}) \cdot \boldsymbol{z}_{i-1} = (\boldsymbol{p}' - \boldsymbol{p}_{i-1}) \tag{7} $$

- distance a_i between the origins $\boldsymbol{p}'$ and $\boldsymbol{p}_i$ (length of the common normal)

$$ a_i = (\boldsymbol{p}_i - \boldsymbol{p}_{i-1}) \cdot \boldsymbol{x}_i = (\boldsymbol{p}_i - \boldsymbol{p}') \tag{8} $$

- angle α_i between z-axes $\boldsymbol{z}_{i-1}$ and $\boldsymbol{z}_i$ around x-axis $\boldsymbol{x}_i$ (the common normal)

$$ \alpha_i = \mathrm{atan2}\left((\boldsymbol{z}_{i-1} \times \boldsymbol{z}_i) \cdot \boldsymbol{x}_i), (\boldsymbol{z}_{i-1} \cdot \boldsymbol{z}_i\right) \tag{9} $$

Using Eqs. (6)–(9) we can compute only the DH parameter sets $(a_i, \alpha_i, d_i, \theta_i), i = 1,\dots,n-1$. The last set of parameters $(a_n, \alpha_n, d_n, \theta_n)$ can be computed using (1). Indeed, it is reasonably assumed that one knows ${}^{n}\mathbf{T}_E$. Assuming that the position of the end-effector frame $\mathcal{F}_E$ described by ${}^{0}\mathbf{T}_E$ is also known and using the transformation matrices ${}^{i-1}\mathbf{T}_i$ obtained earlier, we obtain

$$ {}^{n-1}\mathbf{T}_n(a_n, \alpha_n, d_n, \theta_n) = \left(\prod_{i=1}^{n} {}^{i-1}\mathbf{T}_i(q_i)\right)^{-1} {}^{0}\mathbf{T}_E \left({}^{n}\mathbf{T}_E\right)^{-1}\,. \tag{10} $$

As ${}^{n-1}\mathbf{T}_n$ has the form given in (3), the nth DH parameter set can be calculated directly form ${}^{n-1}\mathbf{T}_n$.

3.1.1. Determination of joint axes

As proposed by several authors [13,20,21], the rotation axis for revolute joints can be easily determined by rotating only one joint at a time. By measuring the 3D spatial position of a point, we obtain a set of 3D points in space $\boldsymbol{p}_i, i = 1,\dots,n$. The obtained data set of points is then fitted to a circle (see Fig. 2).

Among various available methods [13,20,22] we used a common approach based on singular value decomposition (SVD). Let the plane $\mathcal{P}$ be represented by a normal $\boldsymbol{n}$ and an arbitrary point on the plane $\boldsymbol{p}_p$. Without loss of generality, we can use as a point on the plane the centroid of all points

$$ \boldsymbol{p}_p = \frac{1}{n}\sum_{i=1}^{n} \boldsymbol{p}_i\,. \tag{11} $$

To find the normal, we have to minimize the orthogonal distance between the set of points and the plane $\mathcal{P}$

$$ \boldsymbol{h}_i = (\boldsymbol{p}_i - \boldsymbol{p}_p) \cdot \boldsymbol{n}\,. \tag{12} $$

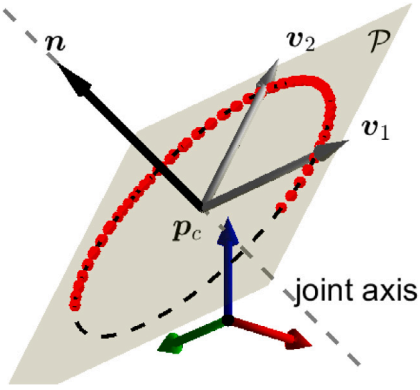

Fig. 2. Captured 3D points (red dots) defining a circle, center point and normal. (For interpretation of the references to color in this figure legend, the reader is referred to the web version of this article.)

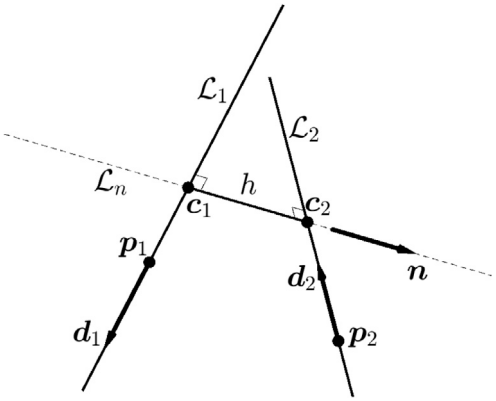

Fig. 3. Two skewed lines in 3D space.

Using the Frobenius norm we define the problem as

$$\boldsymbol{n} = \arg\max_{\boldsymbol{n}} \|\mathbf{P}\boldsymbol{n}\|^2 , \tag{13}$$

where

$$\mathbf{P} = \begin{bmatrix} \boldsymbol{p}_1 - \boldsymbol{p}_p \\ \vdots \\ \boldsymbol{p}_n - \boldsymbol{p}_p \end{bmatrix} . \tag{14}$$

Using SVD we can factorize $\mathbf{P}$ into

$$\mathbf{P} = \mathbf{U}\mathbf{\Sigma}\mathbf{V}^T , \tag{15}$$

where $\mathbf{\Sigma}$ ia a diagonal matrix with singular values $\sigma_i, i, \dots, 3$, in decreasing order. As $\mathbf{U}$ is a unitary matrix, the problem (13) reduces to

$$\boldsymbol{n} = \arg\max_{\boldsymbol{n}} \|\mathbf{\Sigma}\mathbf{V}^T\boldsymbol{n}\|^2 = \arg\max_{\boldsymbol{n}} \sum_{i=1}^{3} \sigma_i (\mathbf{V}^T\boldsymbol{n})_i . \tag{16}$$

As the smallest singular value in $\mathbf{\Sigma}$ is the last component σ_3, the solution is

$$\boldsymbol{n} = \mathbf{V}[0, 0, 1]^T \tag{17}$$

Finally, we must check whether the normal is in the correct direction of the joint axis and correct it if necessary

$$\boldsymbol{n} = \begin{cases} \boldsymbol{n} , & \text{for } \boldsymbol{n} \cdot (\boldsymbol{p}_1 \times \boldsymbol{p}_2) \geq 0 \\ -\boldsymbol{n} , & \text{for } \boldsymbol{n} \cdot (\boldsymbol{p}_1 \times \boldsymbol{p}_2) < 0 \end{cases} \tag{18}$$

where we use two points from the acquired data set, $\boldsymbol{p}_1(\boldsymbol{q}_1)$ and $\boldsymbol{p}_2(\boldsymbol{q}_2)$, so that the rotation from $\boldsymbol{q}_1$ to $\boldsymbol{q}_2$ is a rotation in the positive direction.

Next, we determine the circle that best fits the captured points. It is convenient to analyze the points in the coordinate frame defined by the orthogonal vectors $\boldsymbol{v}_1$, $\boldsymbol{v}_2$, and $\boldsymbol{n}$. Projecting the captured points to the plane $\mathcal{P}$ using the mapping

$$[x_i, y_i] = \boldsymbol{p}_i[\boldsymbol{v}_1, \boldsymbol{v}_2] \tag{19}$$

we reduce the fitting problem to a two-dimensional problem. In (19), the vectors $\boldsymbol{v}_1$ and $\boldsymbol{v}_2$ are respectively the first two columns of $\mathbf{V}$. From the obtained points on the plane $[x_i, y_i], i, \dots, n$, the best fitting circle can be easily determined. A 2D circle with center $[x_c, y_c]$ and radius r is represented as

$$(x - x_c)^2 + (y - y_c)^2 = r^2 \tag{20}$$

Rearranging this to a function of x and y yields

$$(x^2 + y^2)\frac{1}{a} - 2x\frac{x_c}{a} - 2y\frac{y_c}{a} = 1, \qquad a = r^2 - x_c^2 - y_c^2 \tag{21}$$

Using (21) for all projected points we get a system of linear equations in form

$$\mathbf{A}\boldsymbol{x} = \boldsymbol{b} \tag{22}$$

where

$$\mathbf{A} = \begin{bmatrix} (x_1^2 + y_1^2) & -2x_1 & -2y_1 \\ \vdots & \vdots & \vdots \\ (x_n^2 + y_n^2) & -2x_n & -2y_n \end{bmatrix}, \quad \boldsymbol{x} = \frac{1}{a}\begin{bmatrix} 1 \\ x_c \\ y_c \end{bmatrix}, \quad \boldsymbol{b} = \mathbf{1}_{1\times n} \tag{23}$$

The solution of (22) in a least-squares sense is

$$\boldsymbol{x} = (\mathbf{A}^T\mathbf{A})^{-1}\mathbf{A}^T\boldsymbol{b} \tag{24}$$

From $\boldsymbol{x}$, $\boldsymbol{x} = [x_1, x_2, x_3]^T$, we get the circle center

$$x_c = \frac{x_2}{x_1} , \qquad y_c = \frac{x_3}{x_1} \tag{25}$$

and the circle radius

$$r = \sqrt{\frac{1}{x_1} + x_c^2 + y_c^2} \tag{26}$$

Finally, we calculate the 3D circle center as

$$\boldsymbol{p}_c = \boldsymbol{p}_p + [\boldsymbol{v}_1, \boldsymbol{v}_2]\begin{bmatrix} x_c \\ y_c \end{bmatrix} . \tag{27}$$

Point $\boldsymbol{p}_c$ and normal $\boldsymbol{n}$ define the location and the direction of the joint axis in 3D space, respectively.

3.1.2. Spatial position of two lines

In general, two lines in 3D space intersect, are parallel, collinear, or skewed to each other. There are several methods to determine their relationship and the intersection or nearest points. In [23] a method based on dual vector algebra is presented. A similar approach using Plücker coordinates is presented in [13,24]. In [25], the problem is solved using constraint optimization to find the minimum distance between lines. A closed form solution can be obtained using a geometric approach [26]. Any of the proposed methods can be used to determine the closest points on two lines. In our work, we use the geometric approach.

Consider two 3D lines as shown on Fig. 3 defined by a point $\boldsymbol{p}$ and a unit direction vector $\boldsymbol{d}$ as

$$\begin{aligned} \mathcal{L}_1 : \quad & \boldsymbol{c}_1(\lambda_1) = \boldsymbol{p}_1 + \lambda_1\boldsymbol{d}_1 \\ \mathcal{L}_2 : \quad & \boldsymbol{c}_2(\lambda_2) = \boldsymbol{p}_2 + \lambda_2\boldsymbol{d}_2 \end{aligned} \tag{28}$$

For these two line we need to find the distance h between them and the closest points $\boldsymbol{c}_1$ and $\boldsymbol{c}_2$. The distance is minimal when the line $\mathcal{L}_n$

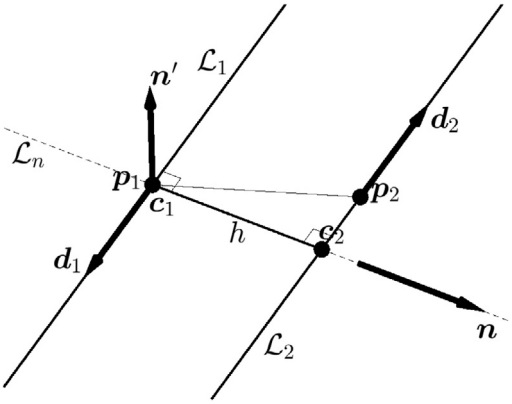

Fig. 4. Two parallel lines in 3D space.

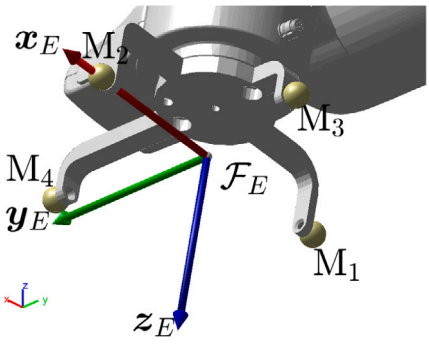

Fig. 5. A tool with four markers attached to the robot end-effector. Frame $\mathcal{F}_E$ defines the robot end-effector pose.

connecting these two points is perpendicular to both lines. This means that the following two conditions have to be satisfied

$$\begin{aligned} \boldsymbol{d}_1 \cdot (\boldsymbol{c}_2 - \boldsymbol{c}_1) = 0 \\ \boldsymbol{d}_2 \cdot (\boldsymbol{c}_2 - \boldsymbol{c}_1) = 0 \end{aligned} \tag{29}$$

Inserting (28) into (29) yields two linear equations

$$\begin{aligned} \boldsymbol{d}_1 \cdot (\boldsymbol{p}_2 - \boldsymbol{p}_1 + \lambda_2 \boldsymbol{d}_2 - \lambda_1 \boldsymbol{d}_1) = 0 \\ \boldsymbol{d}_2 \cdot (\boldsymbol{p}_2 - \boldsymbol{p}_1 + \lambda_2 \boldsymbol{d}_2 - \lambda_1 \boldsymbol{d}_1) = 0 \end{aligned} \tag{30}$$

Solving them for λ_1 and sL_2 yields

$$\lambda_1 = \frac{a_1 n_2 - a_2 n_{12}}{d}, \qquad \lambda_2 = \frac{\lambda_1 n_{12} - a_2}{n_2} \tag{31}$$

where

$$\begin{aligned} n_1 = \boldsymbol{d}_1^T \boldsymbol{d}_1, \quad n_2 = \boldsymbol{d}_2^T \boldsymbol{d}_2, \quad n_{12} = \boldsymbol{d}_1^T \boldsymbol{d}_2, \\ a_1 = \boldsymbol{d}_1^T (\boldsymbol{p}_2 - \boldsymbol{p}_1), \quad a_2 = \boldsymbol{d}_2^T (\boldsymbol{p}_2 - \boldsymbol{p}_1) \\ d = n_1 n_2 - n_{12}^2 \end{aligned} \tag{32}$$

Having the solution for location of closest points λ_1 and λ_2, the distance between lines is calculated as

$$\boldsymbol{h} = \|\boldsymbol{c}_2 - \boldsymbol{c}_1\| = \|\lambda_2 \boldsymbol{d}_2 - \lambda_1 \boldsymbol{d}_1 + \boldsymbol{p}_2 - \boldsymbol{p}_1\| \tag{33}$$

When the points $\boldsymbol{c}_1$ and $\boldsymbol{c}_2$ coincide, the lines are intersecting and $h = 0$.

When $\|\boldsymbol{d}_1 \times \boldsymbol{d}_2\| = 0$ the two lines are parallel. For parallel lines, there is no unique solution for a common normal. A solution can be determined by choosing a point on a line through which the common normal passes. Let $\boldsymbol{c}_1$ be the selected point on $\mathcal{L}_1$ (see Fig. 4). Then we define an auxiliary normal vector using any point on $\mathcal{L}_2$

$$\boldsymbol{n}' = (\boldsymbol{p}_2 - \boldsymbol{p}_1) \times \boldsymbol{d}_1 . \tag{34}$$

Next, the normal $\boldsymbol{n}$ is calculated as

$$\boldsymbol{n} = \frac{\boldsymbol{n}' \times \boldsymbol{d}_1}{\|\boldsymbol{n}'\|} . \tag{35}$$

Now it is straightforward to calculate the distance between lines

$$\boldsymbol{h} = (\boldsymbol{p}_2 - \boldsymbol{p}_1) \cdot \boldsymbol{n} \tag{36}$$

and the point $\boldsymbol{c}_2$ on $\mathcal{L}_2$

$$\boldsymbol{c}_2 = \boldsymbol{c}_1 + h\boldsymbol{n} . \tag{37}$$

Points $\boldsymbol{c}_1$ and $\boldsymbol{c}_2$ are then used in Eqs. (7) and (8) as the points $\boldsymbol{p}'$ and $\boldsymbol{p}_i$, respectively.

3.2. Optimization approach

Another approach to estimating DH parameters is to use an optimization method [27,28]. In this case, we try to find the best estimate of the DH parameters that minimizes an objective function. By measuring the robot configurations, i.e., joint positions $\boldsymbol{q}$, we can compute the end-effector poses using forward kinematics $\{\boldsymbol{p}_E, \mathcal{Q}_E\}$. The differences between the measured real end-effector positions $\{\boldsymbol{p}_M, \mathcal{Q}_M\}$ and the calculated ones represent errors of the robot model and are used as objective functions in the optimization process. Thus, we define the optimization problem as

$$\mathrm{DH} = \arg\min_{\mathrm{DH}} \sum_{i=1}^{m} \left(\|\boldsymbol{p}_E(\boldsymbol{q}_i, \mathrm{DH}) - \boldsymbol{p}_{M,i}\| + \mu \|2 \log(\mathcal{Q}(\boldsymbol{q}_i, \mathrm{DH}) \mathcal{Q}_{M,i}^{-1})\| \right) , \tag{38}$$

where μ is the scaling factor between the position and orientation error norms and m is the number of data samples measured. A good choice for the initial values of the DH parameters are the values of the nominal DH parameters.

3.3. Validation of estimation methods

To validate the proposed method for estimating DH parameters, we used a model of the Franka Emika Panda robot in the Haptix simulation environment based on the general-purpose physics engine MuJoCo, [29].

As explained in Section 3, to identify the DH parameters, the axes of rotation of all joints must be determined. It is not difficult to see that all rotational axes of a robot can be identified by measuring only the position of an appropriate point on the end-effector while one joint is moving and all other joints are fixed in any position. Note that it is not even necessary to know the exact position of this point on the robot body. The only requirement is that the measurement point is not on the axis of rotation. An exception is the last set of DH parameters. To identify this set, it is necessary to measure the position and orientation of the end-effector.

We defined a rigid body with four simulated markers. This object was attached to the end-effector of the robot. The frame of the end-effector was determined using the markers, as shown in Fig. 5. In Haptix, we used sensors that measured the position of the four markers and the pose of the frame $\mathcal{F}_E$.

To obtain a circular motion, we defined trajectories in which only one joint moved at a time. The range of motion included as much of the available joint range as possible. During this motion, the other joints were in fixed positions. The resulting circles and normals to circular planes used to calculate the DH parameters are shown in Fig. 6. Using the circle centers and normals as input to the method described in Section 3.1, we obtained the DH parameters of the robot model. As expected, they correspond to the nominal values given by the robot manufacturer for both methods (geometric and optimization) and are given in Table 2.

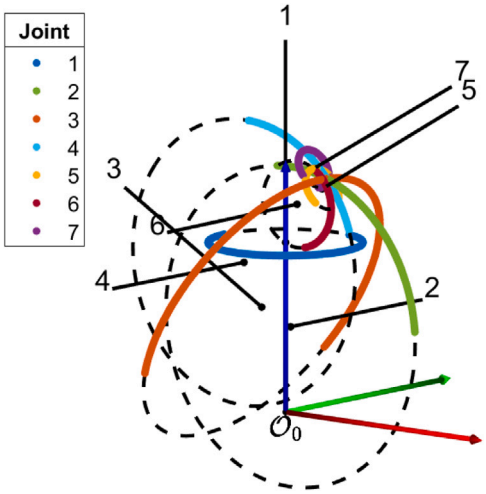

Fig. 6. Measured circles and normals for all joints using Haptix simulation.

Table 2
Nominal DH parameters of Franka Emika Panda robot.

Joint	a [mm]	d [mm]	α [deg]	θ [deg]
1	0	333	−90	0
2	0	0	90	0
3	82.5	316	90	0
4	−82.5	0	−90	0
5	0	384	90	0
6	88	0	90	0
7	0	107	0	0

3.3.1. Estimation reliability

When calculating the kinematic model parameters for a real robot, it is important to know the accuracy of the obtained DH parameters. From the equations in Section 3.1.1 it follows that only the position of points (markers) on the robot end-effector is important for the estimation of joint axes. Thus, the key factor affecting the accuracy of the parameters is the accuracy of the external system used to measure the position of the end-effector. Theoretically, the position of a point on the end-effector is always on a plane when only one rotary joint is moving. In other words, the position component in the direction of the plane normal $\boldsymbol{n}$ is 0. In practice, the points are not in the plane because of the measurement noise, elasticity of the robot structure or mechanical tolerances in gears (if the motion is such that the gravity influences are changing during the motion).

To quantify the deviation of the measured points from the circular plane, we propose a quality measure using the singular values obtained from (15)

$$\xi = \sigma_3 \max(\boldsymbol{U}_3) \tag{39}$$

where σ_3 is the smallest singular value and $\max(\boldsymbol{U}_3)$ is the maximum value of the components in the corresponding column of the matrix $\mathbf{U}$. Note that ξ is the maximum position deviation of the measured points in the direction $\boldsymbol{n}$.

In simulation, it is easy to change the noise level of the marker position measurement and then estimate the sensitivity of the DH parameters to the inaccuracy of the marker position. So we added noise with normal (Gaussian) distribution $N(0, \sigma_N)$ to the marker position measurement. We ran a series of simulations in which we changed the level of noise $\sigma_N = [0, \ldots, 1\ \text{mm}]$). For each σ_N, we repeated the whole estimation procedure 50 times. First, we analyzed the effect of measurement noise on the quality measure ξ. In Fig. 7, we can see that ξ depends linearly on the noise level (for normally distributed noise, the maximum deviation in the $\boldsymbol{n}$ direction is about three times the standard deviation).

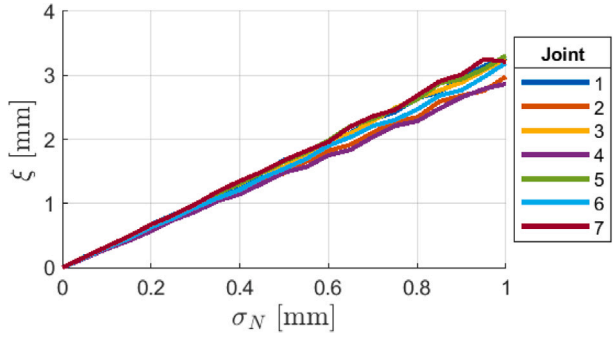

Fig. 7. Measurement quality measure ξ versus the marker position measurement noise (σ_N).

Next, we checked the influence of measurement noise on the calculation of DH parameters. Fig. 8 shows the standard deviation of the DH parameters as a function of the noise level. We can see that the reliability of the calculated DH parameters is in the range of the measurement noise.

4. Experimental identification of DH parameter

The objective was to verify that the DH parameters of the Franka Emika Panda collaborative robot conform to specifications. To estimate the kinematic model parameters of the robot, the joint positions and the poses in the task space have to be measured.

Additionally, we wanted to show, that it is possible to calibrate a robot in its working environment. Therefore, we used a robot mounted on a mobile platform. Although, the mobile platform was not supposed to move during the calibration process, some motion of the mobile platform and the robot mounting plate can occur due to the mechanical structure of the whole system (e.g., due to the wheel suspension). Therefore, we measured not only the pose of the robot end-effector but also the pose of the robot base.

4.1. Experimental setup

Our experimental setup consists of a Franka Emika Panda robot mounted on a plate on a mobile platform PAL Tiago-base. To measure the position of the robot base, we mounted six markers on the plate. The robot was equipped with a specially designed tool with markers attached to the end-effector. As an external measurement system, we used an optical motion capture system (MoCap), as shown in Fig. 9. The robot is controlled by a control system based on Matlab and ROS, which allows easy motion programming and the acquisition of robot states.

The actual pose of the tool in Cartesian space was measured using the MoCap system. More specifically, we used a passive marker-based OptiTrack system that can localize the positions of markers and track their motion in space in real time. Our MoCap system consists of 16 Prime 13 W IR cameras, which are arranged throughout the space to cover a measurement range larger than the robot's working range. In experiment we use ten markers with diameter 14 mm, which are placed on the robot base and on the robot tool. When properly calibrated, the OptiTrack system has a marker position measurement accuracy of better than +/−0.3 mm in the measurement volume [30,31]. It can capture marker positions at a rate of up to 240 Hz.

With the OptiTrack system, a rigid body can be defined as a collection of three or more fixed markers on an object connected to each other, where the distance from marker to marker does not deviate beyond the allowable tolerance. With a rigid body, the system can measure the pose (position and orientation) with better accuracy (up to +/−0.15 mm).

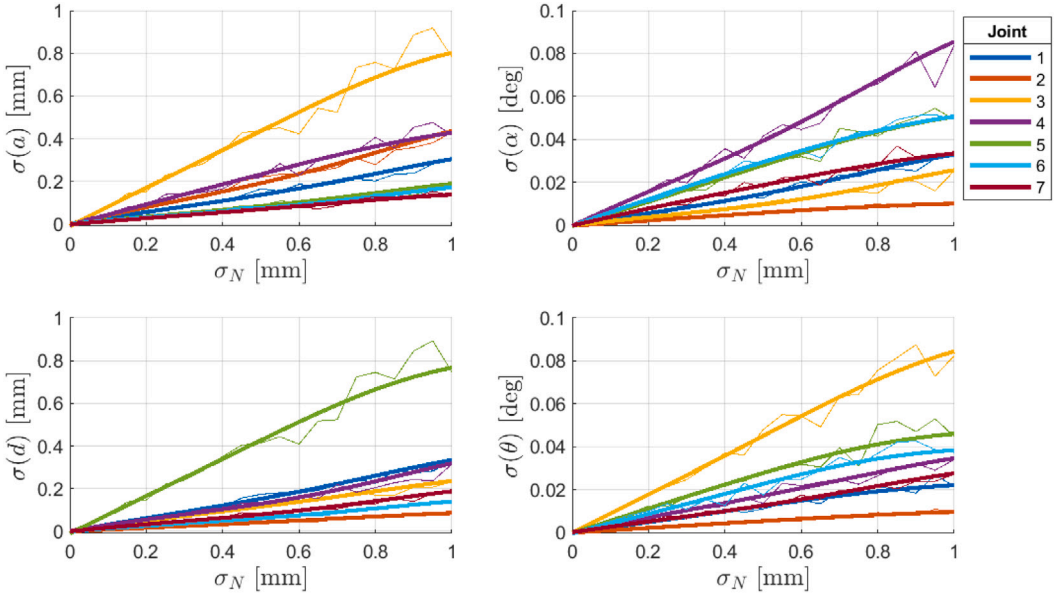

Fig. 8. Standard deviation of calculated DH parameters versus the marker position measurement noise (σ_N) (thicker lines are the trends) — Note that the worst camera reprojection of used MoCap system was up to 0.373 mm.

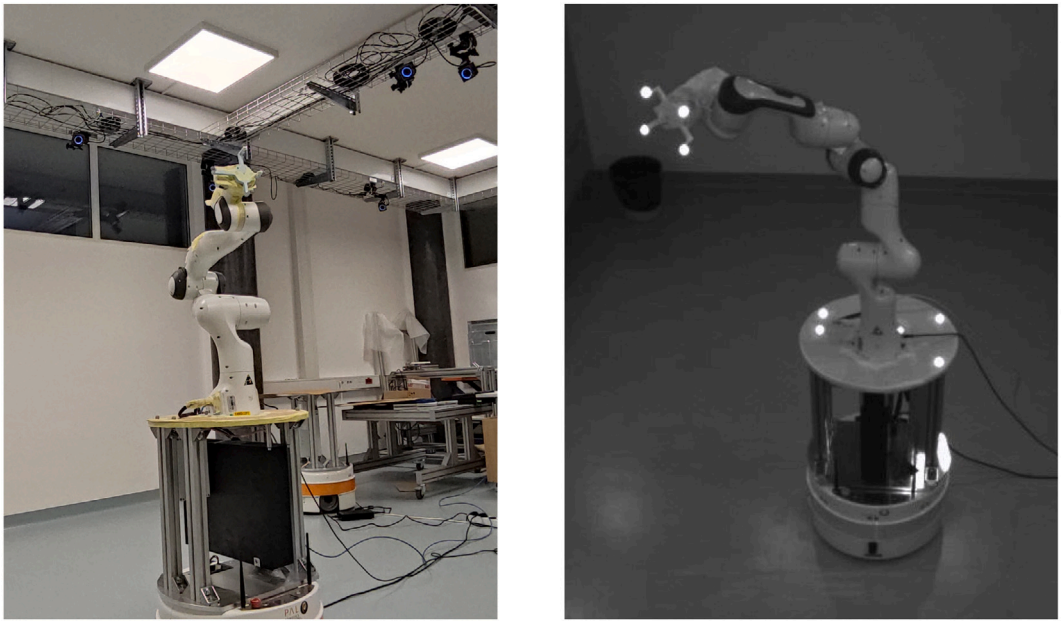

Fig. 9. MoCap scene: Franka Emika Panda with marker tool (left), IR image captured by MoCap camera (right).

4.2. Mapping between optical and robot frame

To estimate the kinematic model, we need to determine the position of the robot end-effector in the robot frame, which is generally aligned with the robot base. During the calibration of the MoCap system, we determine the optical frame that can be used as the world frame without loss of generality. Since this frame $\mathcal{F}_W$ is not aligned with the robot frame, we need to define the mapping between the world frame and the robot frame.

To determine the position of the robot base in world space we have equipped the robot base with six markers at specific positions (see Fig. 10) and defined a MoCap virtual rigid-body. These markers were used to determine the position of the robot base (origin of $\mathcal{F}_0$). Using the positions of the markers M_1, M_2, M_5 and M_6 as input for Eqs. (11)–(17), we obtain the plane of the robot base $\mathcal{P}_0$ and its normal z_0. The markers M_3 and M_4, placed on two precision holes of the robot mounting plate (parallel to the base plane), determine the position p_0 and the rotation of the robot base

$$\begin{aligned} \boldsymbol{y}_0 &= \frac{\boldsymbol{p}_{M_4} - \boldsymbol{p}_{M_3}}{\|\boldsymbol{p}_{M_4} - \boldsymbol{p}_{M_3}\|} \\ \boldsymbol{x}_0 &= \boldsymbol{y}_0 \times \boldsymbol{z}_0 \\ \boldsymbol{p}_0 &= \frac{\boldsymbol{p}_{M_3} + \boldsymbol{p}_{M_4}}{2} \begin{bmatrix} 1 & 0 & 0 \\ 0 & 1 & 0 \\ 0 & 0 & 0 \end{bmatrix} + b\boldsymbol{x}_0 \end{aligned} \tag{40}$$

where b is the offset of the robot frame origin from the precision holes. Since the robot manufacturer did not specify this offset we had to estimate its value.

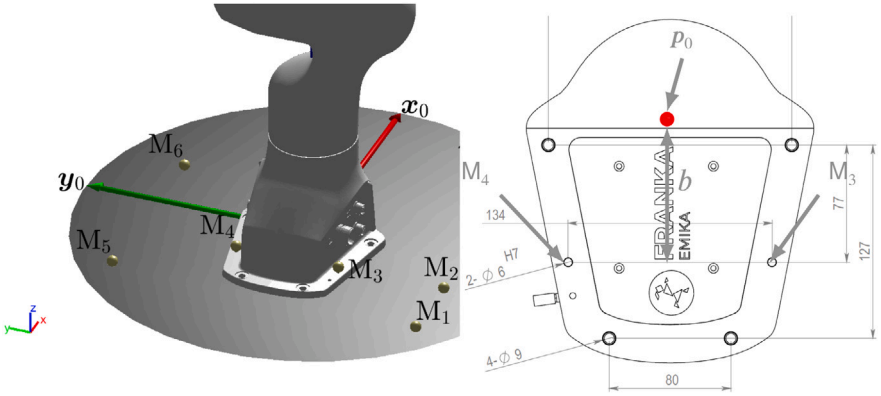

Fig. 10. Markers and body frame on robot base (left); Robot footprint with location of markers M_3 and M_4 locations and robot base origin p_0 (right).

Then, the captured positions ${}^{W}\boldsymbol{p}$ can be mapped to robot frame using

$$ {}^{0}\boldsymbol{p} = {}^{0}\mathbf{T}_{W}\, {}^{W}\boldsymbol{p} \tag{41} $$

where the transformation matrix representing the mapping from world frame $\mathcal{F}_W$ to robot base frame $\mathcal{F}_0$ is defined as

$$ {}^{0}\mathbf{T}_{W} = \begin{bmatrix} \boldsymbol{x}_0 & \boldsymbol{y}_0 & \boldsymbol{z}_0 & \boldsymbol{p}_0 \\ 0 & 0 & 0 & 1 \end{bmatrix}^{-1} \tag{42} $$

Note that the marker positions used to calculate ${}^{0}\mathbf{T}_{W}$ are defined in the world frame.

In addition, we can check the position of the robot frame $\boldsymbol{p}_0$ and the orientation of the axis $\boldsymbol{z}_0$ using the rotation axis of the first joint $\boldsymbol{a}_1$ and correct it if necessary. Namely, the intersection of the rotation axis of the first joint with the base plane $\mathcal{P}_0$ is the correct origin of the robot base, and the rotation axis of the first joint $\boldsymbol{a}_1$ must be aligned with the z axis of the frame $\mathcal{F}_0$. If this is not the case, then the transformation matrix ${}^{0}\mathbf{T}_{W}$ has to be corrected

$$ {}^{0}\mathbf{T}'_{W} = \begin{bmatrix} {}^{0}\mathbf{R}'_0 & {}^{0}\boldsymbol{p}'_0 \\ \mathbf{0} & 1 \end{bmatrix}^{-1} {}^{0}\mathbf{T}_{W} \tag{43} $$

where ${}^{0}\boldsymbol{p}'_0$ is the intersection of the joint axis $\boldsymbol{a}_1$ with the plane $\mathcal{P}_0$, expressed in the frame $\mathcal{F}_0$, and ${}^{0}\mathbf{R}'_0$ is the rotation matrix that rotates the axis $\boldsymbol{z} = [0, 0, 1]^T$ so that it is aligned with $\boldsymbol{a}_1$, which can be calculated using Rodrigues' rotation formula

$$ {}^{0}\mathbf{R}'_0 = \mathbf{I} + [\boldsymbol{v}]_{\times} + (1 - \cos\varphi)\frac{[\boldsymbol{v}]_{\times}^2}{\|\boldsymbol{v}\|^2}\,, \qquad \boldsymbol{v} = \boldsymbol{z}_0 \times \boldsymbol{a}_1\,, \qquad \cos\varphi = \boldsymbol{z}_0 \cdot \boldsymbol{a}_1\,, \tag{44} $$

where $[\cdot]_{\times}$ is a skew-symmetric operator.

In practice, it is not always possible to place markers on the mounting plate in such configuration that they define the pose of the robot frame $\mathcal{F}_0$. Sometimes, it is even not possible to define the base plane $\mathcal{P}_0$ plane. Without known pose of $\mathcal{F}_0$, we cannot estimate DH parameters d_1 and θ_1. In this case, we propose to use markers fixed to the robot base to define an auxiliary frame $\mathcal{F}_A$ and the corresponding transformation matrix ${}^{A}\mathbf{T}_{W}$. Of course, this is not the correct transformation matrix to map from world to robot frame. It has to be augmented with transformation to robot base frame similar as in (43)

$$ {}^{0}\mathbf{T}_{W} = \begin{bmatrix} {}^{A}\mathbf{R}_0 & {}^{A}\boldsymbol{p}_0 \\ \mathbf{0} & 1 \end{bmatrix}^{-1} {}^{A}\mathbf{T}_{W} \tag{45} $$

If we assume that the actual parameters d_1 and θ_1 are equal to the nominal parameters, then we can determine ${}^{0}\boldsymbol{p}_A$ from the rotation axes of the first two joints $\boldsymbol{a}_1$ and $\boldsymbol{a}_2$. As already explained, the rotation axis of the first joint $\boldsymbol{a}_1$ is the z axis of the frame $\mathcal{F}_0$. Assuming that $\boldsymbol{a}_1$ and $\boldsymbol{a}_2$ are not parallel, from (7) follows that ${}^{0}\boldsymbol{p}_A$ is at distance d_1 from the common normal between $\boldsymbol{a}_1$ and $\boldsymbol{a}_2$. Using Eqs. ((28)–(33)) we obtain the closest points $\boldsymbol{c}_1$ and $\boldsymbol{c}_2$ on rotation axes $\boldsymbol{a}_1$ and $\boldsymbol{a}_2$. Then

$$ {}^{A}\boldsymbol{p}_0 = {}^{A}\boldsymbol{c}_1 - d_1\, {}^{A}\boldsymbol{a}_1 \tag{46} $$

where d_1 is the nominal value of DH parameter. The orientation of $\mathcal{F}_0$ can be determined using (6) and nominal value of DH parameter θ_1. When joint axes $\boldsymbol{a}_1$ and $\boldsymbol{a}_2$ are perpendicular the rotation matrix can be calculated as

$$ {}^{A}\mathbf{R}_0 = \left[\left({}^{A}\boldsymbol{a}_2 \times {}^{A}\boldsymbol{a}_1\right)\,,\ \left({}^{A}\boldsymbol{a}_1 \times \left({}^{A}\boldsymbol{a}_2 \times {}^{A}\boldsymbol{a}_1\right)\right)\,,\ {}^{A}\boldsymbol{a}_1 \right] \tag{47} $$

The mobile platform on which the robot was mounted was not supposed to move during the measurements. However, due to the mechanical structure of the mobile platform, there was still a small movement of the robot base relative to the fixed world frame. Fig. 11 shows the position and orientation deviations of the robot base during an experiment. Some small deviations can be observed since the platform is not very rigid. The deviations were larger when the lower (heavier) links are moved. To compensate for these deviations, we calculated the transformation matrix ${}^{0}\mathbf{T}_{W}$ for each sample.

Fig. 11 shows that the measurement noise of the OptiTrack system is below 0.1. This is in accordance with results in [31] where it is reported that OptiTrack system assures measurement precision of motionless markers below 0.1 mm and the average standard deviation below 0.05 mm. Note that Fig. 11 shows the displacement of almost motionless markers (at least the first 50,000 samples).

In the following, we omit the superscripts denoting the frame when the variables are specified in the robot frame.

4.3. Tool object frame

To improve the accuracy of the end-effector pose measurement, we defined another MoCap virtual rigid body with four markers on a custom-designed tool, as shown in Fig. 5. The end-effector frame $\mathcal{F}_E$ was defined at specific positions using the markers

$$ \begin{aligned} \boldsymbol{x}_E &= \frac{\boldsymbol{p}_{M_2} - \boldsymbol{p}_{M_1}}{\|\boldsymbol{p}_{M_2} - \boldsymbol{p}_{M_1}\|} \\ \boldsymbol{y}_E &= \frac{\boldsymbol{p}_{M_4} - \boldsymbol{p}_{M_3}}{\|\boldsymbol{p}_{M_4} - \boldsymbol{p}_{M_3}\|} \\ \boldsymbol{z}_E &= \boldsymbol{x}_E \times \boldsymbol{y}_E \\ \boldsymbol{p}_E &= \frac{(\boldsymbol{p}_{M_1} + \boldsymbol{p}_{M_1})}{2} \end{aligned} \tag{48} $$

The transformation matrix representing the mapping from MoCap rigid-body frame $\mathcal{F}_{Eo}$ to tool frame $\mathcal{F}_E$ is defined as

$$ {}^{E}\mathbf{T}_{Eo} = \begin{bmatrix} \boldsymbol{x}_E & \boldsymbol{y}_E & \boldsymbol{z}_E & \boldsymbol{p}_E \\ 0 & 0 & 0 & 1 \end{bmatrix}^{-1} \tag{49} $$

where the marker positions used to calculate ${}^{E}\mathbf{T}_{Eo}$ are defined in the frame $\mathcal{F}_{Eo}$.

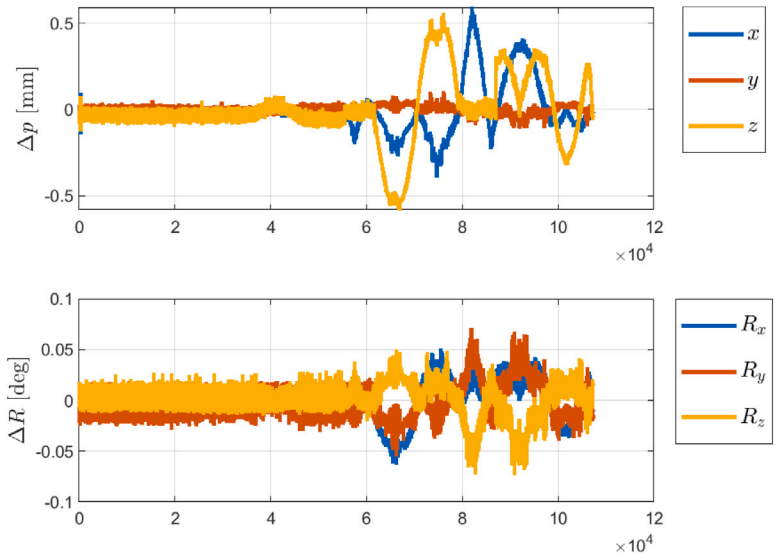

Fig. 11. Example of position and orientation deviation of the robot base during measurement.

4.4. Trajectories

We used three motion schemes to estimate DH parameters in experiments and then verified the identified DH parameters.

For geometric estimation of DH parameters, we generated trajectories in which only one joint moved at a time, resulting in a circular trajectory of the tracked point (referred to as C-trajectories). We have used joint position control strategy. The joint motion occurred at low speed (∼10% of the robot's maximum speed), and the range of motion included almost the entire available joint range. During this motion, the other joints were at fixed positions in an optimal configuration with respect to external influences on measurement accuracy. Fig. 12(a) shows the joint positions for the C trajectory. Due to time scale and faster movements to optimal configuration before each sequence, this can part of motion looks on Fig. 12(a) like a jump in positions.

The second type of motion was used for verification and also for estimation of DH parameters by optimization. The robot moved between 80 random configurations throughout the robot's workspace (referred to as R-trajectory). Fig. 12(b) shows the joint positions for the R-trajectory.

Last, we defined a grid of 42 Cartesian space points with a point-to-point spacing of 0.2 m or 0.3 m distributed in the robot's workspace. The trajectory was defined such that the path passed through all of these points (referred to as the G-trajectory), as shown in Fig. 12(c). At each point, the robot stopped for a short time. This trajectory was also used to verify the improvement in accuracy with the estimated DH parameters.

4.5. Identification of DH parameters using measured data

The geometric approach can only be used for circular C trajectories. From the measured data, we extracted sets of end-effector point motions needed to estimate the position of all joint axes. Each set contained only points at which a joint moved. To minimize the influence of measurement errors of the MoCap system, we measured 3000–14,000 points for each joint, depending on the range of each joint. Fig. 13 shows the acquired points for the circular motion of joint 1 along with the best-fit circle obtained using Eqs. (11)–(27). The acquired points were not in a plane due to measurement noise. Note that the scatter of the points looks larger in the z direction because the scale of the z axis on the figure is not as large as that of the x and y axes. Due to the limitations of the joint, it is not possible to rotate the joint 360 degrees. In our experiments, the joint positions ranged from about 75 degrees for joint 4 to 300 degrees for joint 7. Therefore, the mean position of the acquired points $\boldsymbol{p}_p$ is eccentric with respect to the center of the circle $\boldsymbol{p}_c$. In general, this is not a problem for circle fitting.

Using the acquired data as input to the estimation procedure described in Section 3.1, we calculated the circles and axes for all joints, as shown in Fig. 6. In the next step, we identified the DH parameters (referred to as DH_{GC}). To analyze the influence of measurement noise, the estimation procedure was repeated 16 times for 3 different initial poses (altogether 48 measurements). The final estimated values of DH_{GC} parameters were calculated as the average of all runs. The obtained parameters, their standard deviation, and maximum deviation are given in Table 3.

To verify the improvement in accuracy of task-space positions and orientations we compared the position and orientation difference between the calculated task space poses and the poses captured by MoCap system. When performing R and C trajectories we have used joint position control and for G trajectory the robot was controlled using kinematic controller with redundancy resolution at velocity level. The redundant DOF was used to avoid joint limits. Although the robot has one redundant DOF, this does not influence the validation process. Namely, to calculate the task space pose of the robot end-effector we have captured joint positions and used them as input to the kinematic model based on DH parameters.

The end-effector position error is defined as

$$\Delta\boldsymbol{p}(\mathrm{DH},\boldsymbol{q}) = \|\boldsymbol{p}_E(\mathrm{DH},\boldsymbol{q}) - \boldsymbol{p}_M\| \tag{50}$$

where parameter DH can be the nominal or estimated DH parameters used to calculate the end-effector position, and $\boldsymbol{p}_M$ are captured position of the tool MoCap rigid-body. Similarly, the orientation error is defined as

$$\Delta\mathcal{Q}(\mathrm{DH},\boldsymbol{q}) = \|2\log(\mathcal{Q}(\mathrm{DH},\boldsymbol{q})\mathcal{Q}_M^{-1})\| \tag{51}$$

where $\mathcal{Q}$ and $\mathcal{Q}_M$ are the quaternions representing the calculated and measured orientation of the end-effector, respectively.

Fig. 14 show the comparison of the position and orientation errors for one C, R and G type trajectory obtained by nominal DH parameters and estimated DH_{GC} parameters. The error histogram plots for C trajectory shown in Fig. 14(a) show a significant improvement of position and orientation errors when DH_{GC} parameters are used. For verification we have used the estimated DH_{GC} parameters on R and G trajectories. The error histograms shown in Figs. 14(b) and 14(c) show accuracy improvement. In addition, the 3D error plots in the two figures on the right show the distribution of position errors in the

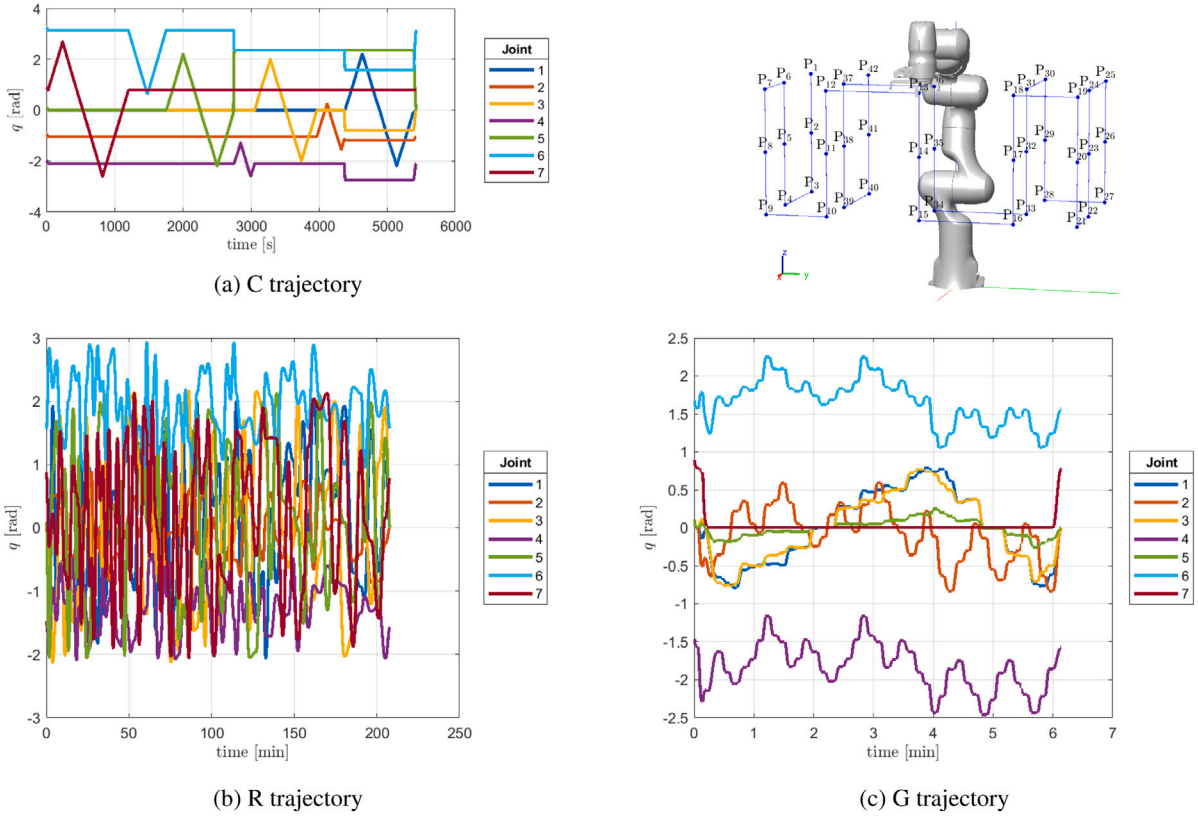

Fig. 12. Three motion schemes. (a) joint trajectory resulting in circular motion of robot end-effector; (b) joint trajectory via random points and (c) task space trajectory via a grid of points.

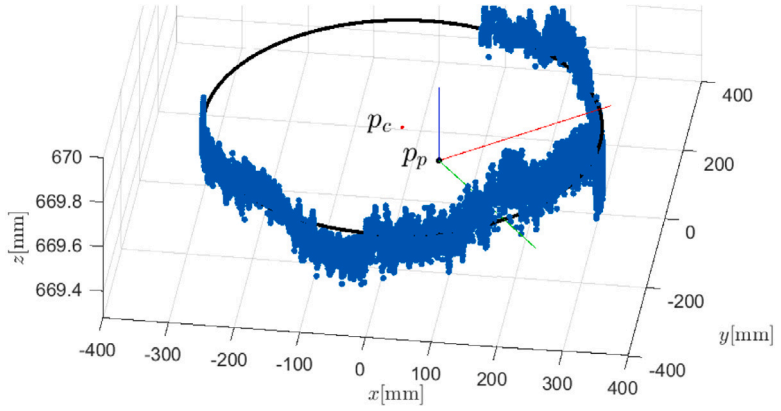

Fig. 13. Captured points and fitted circle for joint 1.

Table 3
Estimated DH_{GC} parameters of Franka Emika Panda robot.

Joint	Mean value				Standard deviation				Maximal deviation			
	a [mm]	d [mm]	α [deg]	θ [deg]	a [mm]	d [mm]	α [deg]	θ [deg]	a [mm]	d [mm]	α [deg]	θ [deg]
1	−0.2	333.0	−90.03	0.00	0.14	0.11	0.020	0.026	0.30	0.23	0.050	0.065
2	0.2	−0.4	89.99	−0.38	0.16	0.06	0.021	0.030	0.32	0.11	0.043	0.054
3	82.3	316.0	89.96	0.27	0.17	0.12	0.012	0.020	0.37	0.23	0.029	0.057
4	−82.6	0.0	−89.98	−0.22	0.13	0.17	0.026	0.011	0.27	0.53	0.065	0.023
5	0.1	384.9	89.63	0.75	0.11	0.17	0.029	0.019	0.21	0.33	0.066	0.041
6	88.0	−0.7	90.07	−0.36	0.05	0.12	0.057	0.035	0.10	0.35	0.117	0.058
7	0.1	107.1	−0.10	−0.29	0.08	0.15	0.058	0.039	0.18	0.31	0.108	0.061

robot's workspace. As we can see, there are some motion parts for the nominal DH parameters where the error is significantly larger. These parts do not depend on the position in the workspace but on the joint configurations. By using the estimated DH_{GC} parameters, the error is

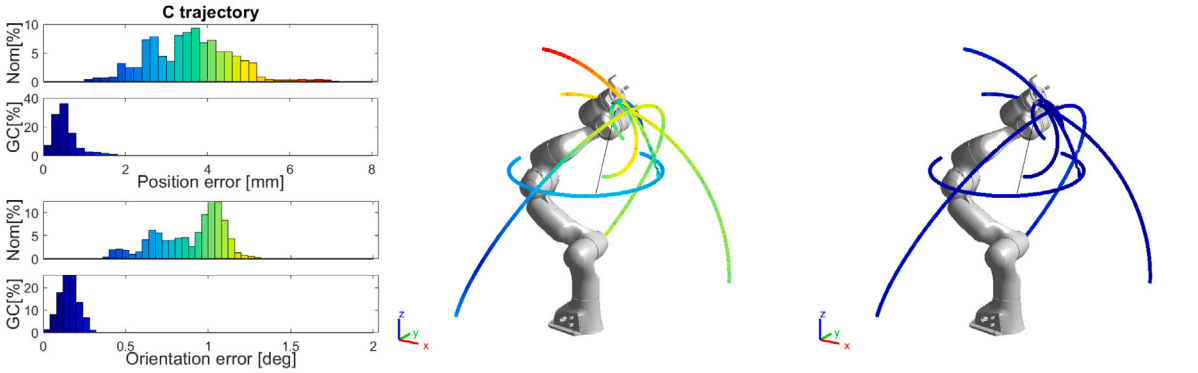

(a) Position and orientation errors with nominal DH and DH_{GC} parameters for C trajectory

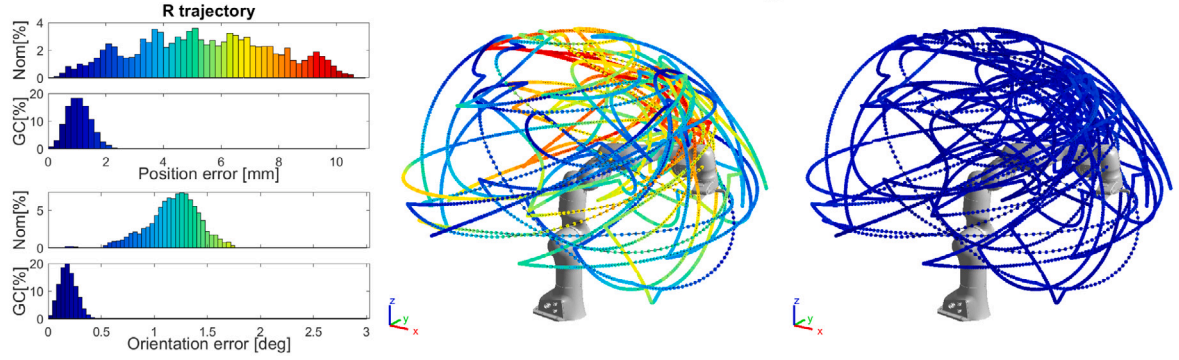

(b) Position and orientation errors with nominal DH and DH_{GC} parameters for R trajectory

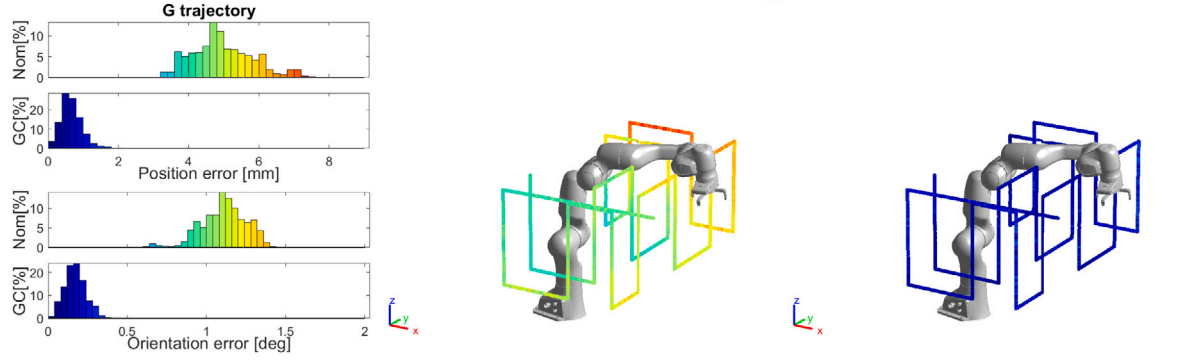

(c) Position and orientation errors with nominal DH and DH_{GC} parameters for G trajectory

Fig. 14. Position and orientation errors with nominal and estimated DH parameters using geometric approach (DH_{GC}) for (a) a C trajectory; (b) an R trajectory; and (c) a P trajectory. The position and orientation error histograms for the acquired points are on the left. The position errors of a subset of the acquired points in the 3D task space are shown for nominal DH parameters in the middle and for DH_{GC} in the right figure (color indicates the magnitude of the error). (For interpretation of the references to color in this figure legend, the reader is referred to the web version of this article.)

improved in all regions. The same improvement can also be seen for G trajectory shown on 3D plots in Fig. 14(c). Note that the standard deviation of the difference between the estimated DH_{GC} parameters and the nominal ones is almost within the accuracy range of the MoCap system (see Table 5).

4.6. Results using optimization

The identification of DH parameters with optimization is independent of the shape of the trajectory, as it only requires simultaneous robot kinematics data and external MoCap measurement data for the robot end-effector pose. Therefore, it is possible to apply the optimization to all three types of trajectories, C, R, and G, respectively. This allows us to determine which trajectory is better for estimating kinematic parameters. Comparing all types of used trajectories, it is obvious that the R trajectory covers the largest part of the robot workspace. Hence, it excites the most different states (see Fig. 12). On the other hand, G trajectory is a representative of a typical motion pattern used for movements in the task space.

We identified the DH parameters by using the measured trajectory data as input to the estimation procedure described in Section 3.2. To analyze the influence of the measurement noise, we used 48 measurements for C, and 16 measurements for R and G type trajectories. The typical time for the optimization for the R trajectory with 300,000 points was 4 h on an i7 processor with 8 cores. We performed optimization for each measurement separately, and the final estimated values of DH parameters were calculated as the average of all runs for each trajectory type. So, we obtained three sets of DH parameters: DH_{OC}, DH_{OR} and DH_{OG}, respectively. For example, the DH_{OR} parameters obtained for R trajectories, their standard deviation, and maximum deviation are given in Table 4. Similar to what was in the case with the geometric approach, the error standard deviation for the estimated DH parameters is also almost within the accuracy range of the MoCap system.

Table 4
Estimated DH_{OR} parameters of Franka Emika Panda robot.

Joint	Mean value				Standard deviation				Maximal deviation			
	a [mm]	d [mm]	α [deg]	θ [deg]	a [mm]	d [mm]	α [deg]	θ [deg]	a [mm]	d [mm]	α [deg]	θ [deg]
1	−0.3	331.6	−90.03	0.01	0.06	0.09	0.007	0.022	0.13	0.25	0.016	0.053
2	0.4	−0.4	90.00	−0.40	0.03	0.04	0.003	0.005	0.06	0.11	0.008	0.012
3	82.6	316.7	89.95	0.31	0.03	0.08	0.004	0.012	0.05	0.14	0.008	0.025
4	−82.5	0.7	−90.01	−0.23	0.03	0.09	0.006	0.003	0.07	0.19	0.012	0.009
5	0.1	385.2	89.65	0.73	0.05	0.07	0.004	0.006	0.11	0.15	0.007	0.010
6	88.1	−0.6	90.05	−0.44	0.05	0.01	0.004	0.002	0.11	0.03	0.007	0.007
7	0.1	106.9	−0.05	−0.20	0.02	0.07	0.002	0.005	0.04	0.17	0.005	0.009

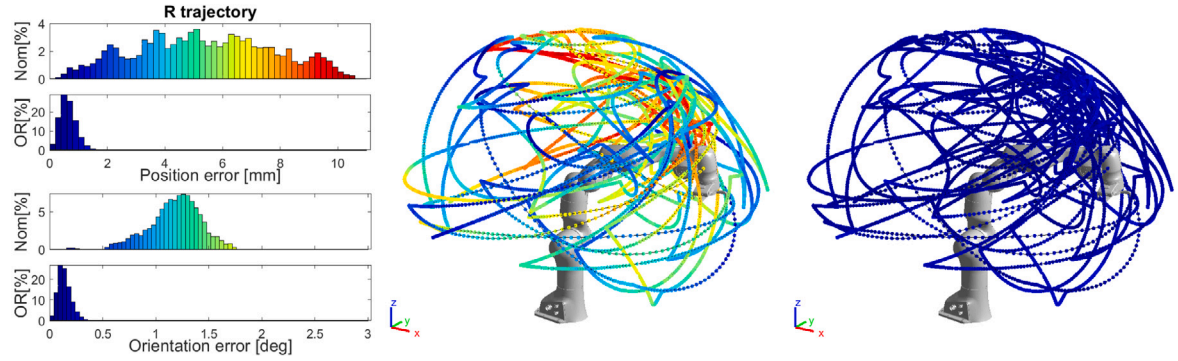

Fig. 15. Position and orientation errors with nominal and optimized DH parameters (DH_{OR}) using R trajectory. Position and orientation error histograms for acquired points are on the left. The position errors of a subset of the acquired points in the 3D task space are shown for nominal DH parameters in the middle and for DH_{OR} in the right figure (color indicates the magnitude of the error). (For interpretation of the references to color in this figure legend, the reader is referred to the web version of this article.)

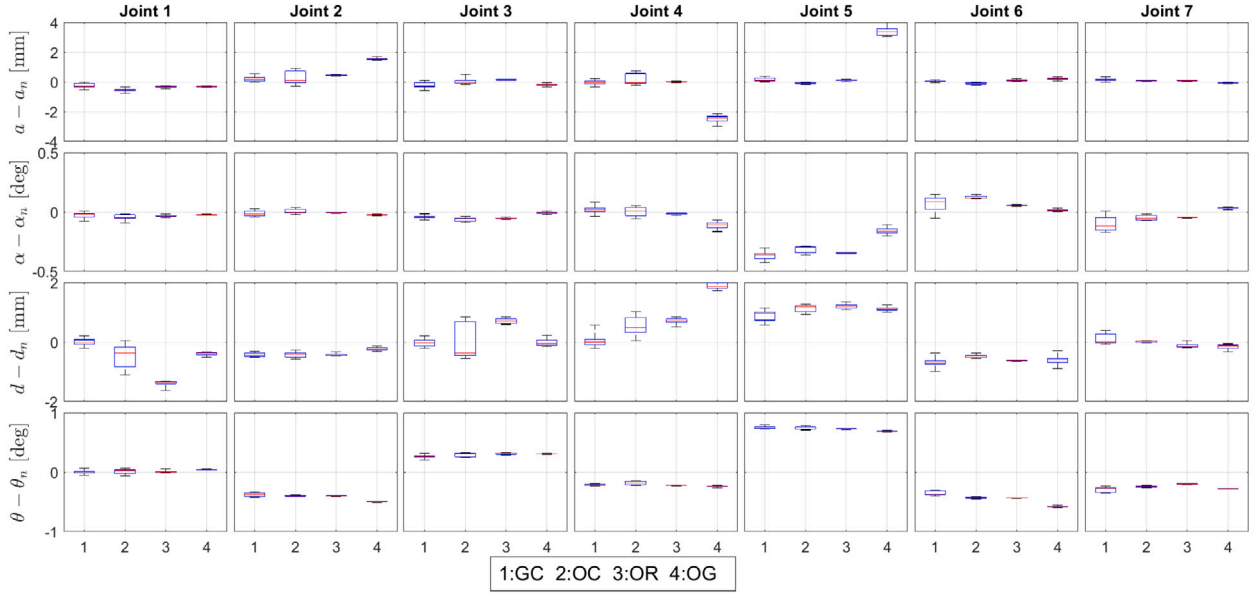

Fig. 16. Deviation of estimated DH parameters from the nominal DH parameters using different methods.

Fig. 15 show the position and orientation errors for one R trajectory obtained by nominal DH parameters and estimated DH_{OR} parameters using optimization, and the position errors along the 3D trajectory. We can see a significant improvement in position and orientation errors when DH_{OR} parameters are used.

5. Discussion

The methods proposed in this paper have been validated with many experiments. In this section we summarize them and highlight the main findings.

Initially, the estimation of kinematic parameters was performed using a typical geometric approach similar to that of [14] but extended with a methodology applicable to robots mounted on a mobile base. The results show that the position and orientation errors were significantly reduced compared to the nominal DH parameters. By analyzing the effects of noise measurement on the identification of DH parameters in Section 3.3.1, we have also shown that the identification quality is within the capabilities of the MoCap measurement system. It is clear that the results obtained with the MoCap system are slightly inferior to other very expensive measurement devices such as laser trackers. Nevertheless, it opens the possibility of using a commonly available measurement device that can also be used online for other possible applications in collaborative robotics [32]. Note that the MoCap system usually has a larger working range and can measure multiple objects simultaneously, which is important when calibrating robots on a mobile

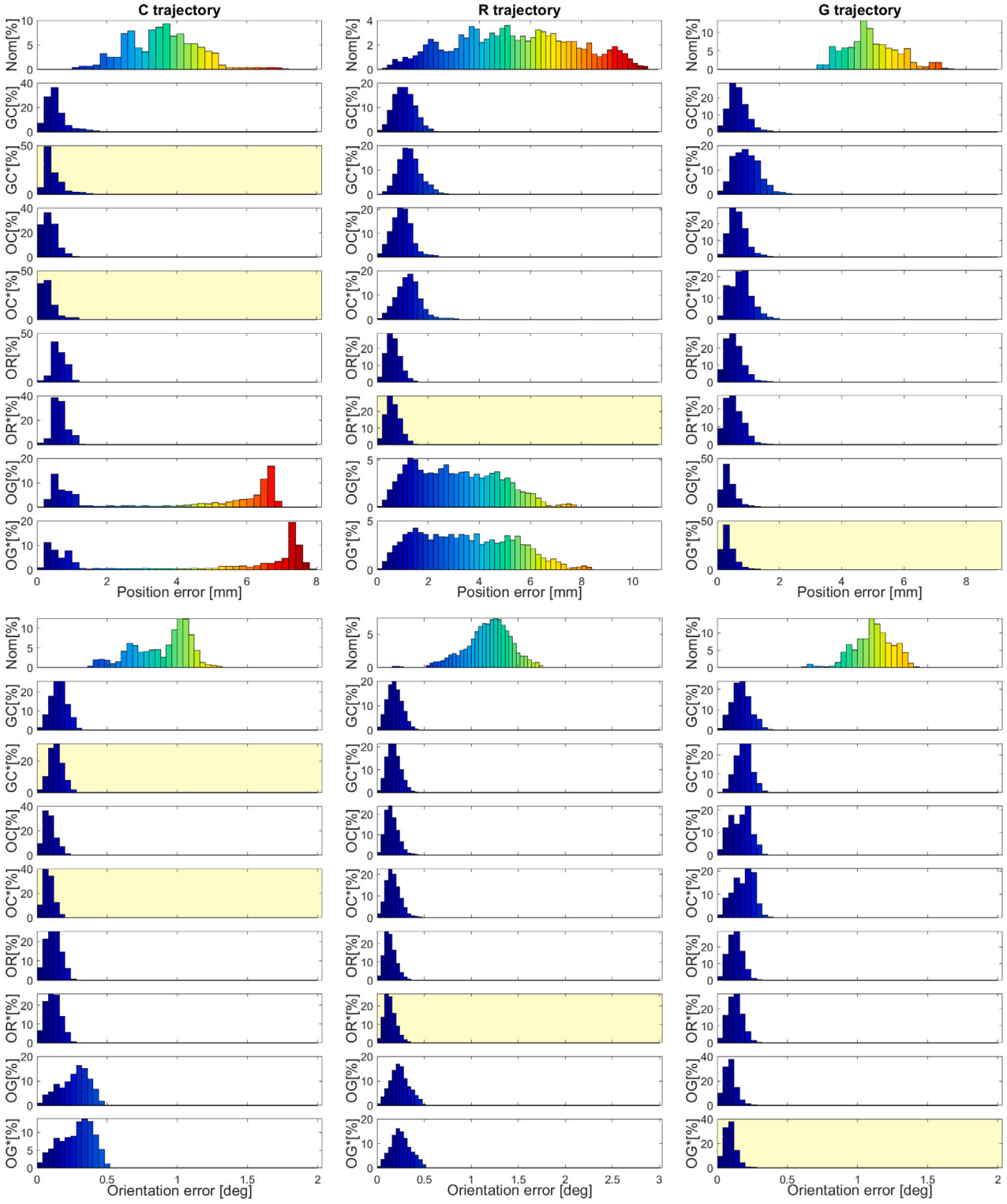

Fig. 17. Comparison of histograms for position errors (upper part) and orientation errors (lower part) for DH parameters obtained by different identification methods (rows) applied to test trajectories (columns): C (left), R (middle), and G (right). (*) and yellow background indicate that DH parameters used were estimated using the same trajectory as for validation. Note that the second and third rows show the results using the DH parameters obtained by the geometric approach, and all others below are obtained by optimization. (For interpretation of the references to color in this figure legend, the reader is referred to the web version of this article.)

platform, when it is necessary to measure simultaneously the robot base and the robot end-effector pose. From the evaluation results it is evident that the approach proposed in this paper significantly improves the accuracy of collaborative robots on a mobile platform by using the corrected (estimated) kinematic model of the robot.

An analysis of the manipulator's workspace was performed using different initial configurations of the robot for identification. The results show that the orientation of the base has a negligible effect on the identification of the DH parameters. We conclude that this is because in our proposed method, the position of the robot base is taken

Table 5
R trajectory: position and orientation errors for nominal and estimated DH parameters using geometric approach and optimization (in [mm] and [deg]).

DH parameters	Δp	$\sigma(\Delta p)$	max(Δp)	ΔQ	$\sigma(\Delta Q)$	max(ΔQ)
DH_{Nom}	5.37	2.36	10.75	1.18	0.24	2.28
DH_{GC}	1.06	0.40	2.54	0.19	0.08	1.40
DH_{OC}	0.96	0.39	2.66	0.16	0.07	1.33
DH_{OR}	0.63	0.27	1.95	0.14	0.06	1.37
DH_{OG}	3.12	1.65	7.89	0.24	0.10	1.33

into account at each step of the measurement, compensating for any movement caused by the robot's own motion.

Fig. 16 shows position and orientation errors for all estimated DH parameters sets that were applied to one trajectory from each set of trajectories. For comparison, the first row shows the results obtained by the nominal DH parameters. Then next two lines present the results for DH_{GC} parameters, and the rest are for optimized DH parameters. For each method we give results for mean values of estimated DH parameters and also for estimated parameters obtained using the particular trajectory, which is used for verification (marked with "*").

For all estimation methods, the position and orientation errors for mean estimated DH parameters applied to one trajectory are slightly worse compared to the errors when DH parameters were used, which were calculated using the same trajectory. The reason is the measurement noise.

When comparing different methods applied to different verification trajectories, we can see the best results are obtained when the same type of trajectory is used for DH parameter estimation and verification. Actually, the error is not significantly worse when the type of trajectory for estimation and verification is not the same. An exception are the DH_{OG} parameters, which were obtained by optimization using G trajectories, which show very bad results for other types of trajectories (last two rows on Fig. 16). The reason is that the G trajectory covers a very limited joint range (see Fig. 12(c)).

On the other side, the overall best results were obtained when the DH parameters were optimized using the R trajectory (DH_{OR}), i.e. optimized DH_{OR} parameters are not very good only for R trajectories but are also very good for other types of trajectories. This is expected as R trajectory has the highest number of points (~300,000 points), which were captured during motion between random points distributed over the entire workspace of the robot. Therefore, R trajectory is the most general set of measured points. In Table 5 we give mean position and orientation errors, their standard deviations, and maximum errors for all acquired points for R trajectory using the nominal DH parameters (DH_{Nom}), estimated DH_{GC} parameters obtained by geometric approach and optimized DH parameters DH_{OC}, DH_{OR} and DH_{OG} are given As already mentioned, the best results were achieved with DH_{OR} parameters (see Fig. 17).

The final accuracy of the robot after using estimated DH parameters presented in this paper is within the range of the MoCap measurement system, regardless of the method used, geometric or optimization. At the same time, the limitation of the geometric approach is that it can only be used for the identification of DH parameters with circular trajectories (C trajectory). In contrast, the optimization approach can be used to identify DH parameters for any trajectory. Additionally, the rule that more is better applies to the optimization approach, which in turn leads to more extended measurements and time-consuming calculations.

6. Conclusion

In this paper, we present two approaches using the MoCap system to determine the DH parameters of a collaborating robot on a mobile platform. Compared to other calibration strategies, such as the use of laser tracker-based systems or mechanical measurement systems, the MoCap measurement system can simultaneously measure both the robot base positions and the end-effector positions. This allows to calibrate robot in its working environment without mounting it on a dedicated basement for calibration. It is also less expensive and more flexible. On the other hand, the main drawback of MoCap systems is that the measurement accuracy is not in the same order of magnitude as a typical laser tracking system. Nevertheless, our presented experimental results with the identified DH parameters show a significant improvement in the position and orientation accuracy. Such improvement in accuracy of calibrated robot allows easier transfer of offline generated motion sequences to a real robot, especially when absolute task space accuracy is essential. We also show that slightly better results are obtained with the optimization approach when a larger data set is used than with the geometric approach. Finally, since the MoCap system allows dynamic simultaneous measurement of many points, it is possible to perform calibration even when the robot base is not fixed.

CRediT authorship contribution statement

Leon Žlajpah: Conceptualization, Methodology, Software. **Tadej Petrič:** Conceptualization, Methodology, Software.

Declaration of competing interest

No author associated with this paper has disclosed any potential or pertinent conflicts which may be perceived to have impending conflict with this work. For full disclosure statements refer to https://doi.org/10.1016/j.rcim.2022.102446.

Data availability

Data will be made available on request.

Acknowledgments

This work was supported by Slovenian Research Agency grant N2-0269 and P2-0076.

References

[1] J.-Q. Xuan, S.-H. Xu, et al., Review on kinematics calibration technology of serial robots, Int. J. Precis. Eng. Manuf. 15 (8) (2014) 1759–1774, http://dx.doi.org/10.1007/s12541-014-0528-1.

[2] Z. Li, S. Li, X. Luo, An overview of calibration technology of industrial robots, IEEE/CAA J. Autom. Sin. 8 (1) (2021) 23–36, http://dx.doi.org/10.1109/JAS.2020.1003381.

[3] M. Vincze, J. Prenninger, H. Gander, A laser tracking system to measure position and orientation of robot end effectors under motion, Int. J. Robot. Res. 13 (4) (1994) 305–314, http://dx.doi.org/10.1177/027836499401300402.

[4] M. Neubauer, H. Gattringer, A. Müller, A. Steinhauser, W. Höbarth, A two-stage calibration method for industrial robots with joint and drive flexibilities, Mech. Sci. 6 (2) (2015) 191–201, http://dx.doi.org/10.5194/ms-6-191-2015.

[5] A. Nubiola, M. Slamani, A. Joubair, I.A. Bonev, Comparison of two calibration methods for a small industrial robot based on an optical CMM and a laser tracker, Robotica 32 (3) (2014) 447–466, http://dx.doi.org/10.1017/S0263574713000714.

[6] A. Nubiola, M. Slamani, I.A. Bonev, A new method for measuring a large set of poses with a single telescoping ballbar, Precis. Eng. 37 (2) (2013) 451–460, http://dx.doi.org/10.1016/j.precisioneng.2012.12.001.

[7] H. Shen, Q. Meng, J. Li, J. Deng, G. Wu, Kinematic sensitivity, parameter identification and calibration of a non-fully symmetric parallel delta robot, Mech. Mach. Theory 161 (2021) http://dx.doi.org/10.1016/j.mechmachtheory.2021.104311.

[8] A.C. Majarena, J. Conte, J. Santolaria, R. Acero, A new methodology for kinematic parameter identification in laser trackers, in: Kinematics, InTech, 2017, http://dx.doi.org/10.5772/intechopen.71444.

[9] A. Brau-Avila, R. Acero, J. Santolaria, M. Valenzuela-Galvan, O. Icasio-Hernández, Kinematic parameter identification procedure of an articulated arm coordinate measuring machine based on a metrology platform, Int. J. Adv. Manuf. Technol. 104 (1–4) (2019) 1027–1040, http://dx.doi.org/10.1007/s00170-019-03878-w.

[10] L. Cheng, W. Wang, Y. Weng, G. Shi, H. Yang, K. Lu, A novel kinematic parameters identification method for articulated arm coordinate measuring machines using repeatability and scaling factor, Math. Probl. Eng. 2018 (2018) http://dx.doi.org/10.1155/2018/1760190.
[11] A.A. Hayat, R.A. Boby, S.K. Saha, A geometric approach for kinematic identification of an industrial robot using a monocular camera, Robot. Comput.-Integr. Manuf. 57 (2019) 329–346, http://dx.doi.org/10.1016/j.rcim.2018.11.008.
[12] J. Gao, H. Han, J. Geng, Z. Li, D. Li, Kinematic parameters identification and compensation of an industrial robot, in: Lecture Notes in Electrical Engineering, vol. 588, Springer Singapore, 2020, pp. 751–766, http://dx.doi.org/10.1155/2021/8874226.
[13] C. Faria, J.L. Vilaça, S. Monteiro, W. Erlhagen, E. Bicho, Automatic denavit-hartenberg parameter identification for serial manipulators, in: IECON 2019 - 45th Annual Conference of the IEEE Industrial Electronics Society, vol. 1, 2019, pp. 610–617, http://dx.doi.org/10.1109/IECON.2019.8927455.
[14] R.A. Boby, A. Klimchik, Combination of geometric and parametric approaches for kinematic identification of an industrial robot, Robot. Comput.-Integr. Manuf. 71 (2021) 102142, http://dx.doi.org/10.1016/j.rcim.2021.102142.
[15] S. He, L. Ma, C. Yan, C.-H. Lee, P. Hu, Multiple location constraints based industrial robot kinematic parameter calibration and accuracy assessment, Int. J. Adv. Manuf. Technol. 102 (5) (2019) 1037–1050, http://dx.doi.org/10.1007/s00170-018-2948-z.
[16] X. Chen, Q. Zhang, Y. Sun, Non-kinematic calibration of industrial robots using a rigid–flexible coupling error model and a full pose measurement method, Robot. Comput.-Integr. Manuf. 57 (2019) 46–58, http://dx.doi.org/10.1016/j.rcim.2018.07.002.
[17] Y. Liu, Y. Li, Z. Zhuang, T. Song, Improvement of robot accuracy with an optical tracking system, Sensors (Switzerland) 20 (21) (2020) 1–26, http://dx.doi.org/10.3390/s20216341.
[18] L. Žlajpah, T. Petrič, Geometric identification of denavit-hartenberg parameters with optical measuring system, in: A. Muller, M. Brandstotter (Eds.), Advances in Service and Industrial Robotics, vol. 120, Springer Nature, Switzerland, 2022, pp. 1–8, http://dx.doi.org/10.1007/978-3-031-04870-8_1.
[19] B. Siciliano, L. Sciavicco, L. Villani, G. Oriolo, Robotics - Modelling, Planning and Control, Springer-Verlag London, 2009, http://dx.doi.org/10.1007/978-1-84628-642-1.
[20] A.A. Hayat, R.G. Chittawadigi, A.D. Udai, S.K. Saha, Identification of denavit-hartenberg parameters of an industrial robot, in: AIR '13, Association for Computing Machinery, New York, NY, USA, 2013, pp. 1–6, http://dx.doi.org/10.1145/2506095.2506121.
[21] M. Abderrahim, A.R. Whittaker, Kinematic model identification of industrial manipulators, Robot. Comput.-Integr. Manuf. 16 (1) (2000) 1–8, http://dx.doi.org/10.1016/S0736-5845(99)00038-1.
[22] D. Umbach, K.N. Jones, A few methods for fitting circles to data, IEEE Trans. Instrum. Meas. 52 (6) (2003) 1881–1885, http://dx.doi.org/10.1109/TIM.2003.820472.
[23] J.S. Ketchel, P.M. Larochelle, Collision detection of cylindrical rigid bodies using line geometry, in: Proceedings of the ASME International Design Engineering Technical Conferences and Computers and Information in Engineering Conference - DETC2005, vol. 7 B, 2005, pp. 811–825, http://dx.doi.org/10.1115/DETC2005-84699.
[24] C. Rajeevlochana, S. Subir, K. Shivesh, Automatic extraction of DH parameters of serial manipulators using line geometry, in: The 2nd Joint International Conference on Multibody System Dynamics, (May) 2012, pp. 1–9.
[25] Y. Pan, L. Iorga, A.A. Pelegri, Numerical generation of a random chopped fiber composite RVE and its elastic properties, Compos. Sci. Technol. 68 (13) (2008) 2792–2798, http://dx.doi.org/10.1016/j.compscitech.2008.06.007.
[26] M. Bailakanavar, Y. Liu, J. Fish, Y. Zheng, Automated modeling of random inclusion composites, Eng. Comput. 30 (4) (2014) 609–625, http://dx.doi.org/10.1007/s00366-012-0310-x.
[27] K.-L. Li, W.-T. Yang, K.-Y. Chan, P.-C. Lin, An optimization technique for identifying robot manipulator parameters under uncertainty, SpringerPlus 5 (1) (2016) 1–16, http://dx.doi.org/10.1186/s40064-016-3417-5.
[28] M. Švaco, B. Šekoranja, F. Šuligoj, B. Jerbić, Calibration of an industrial robot using a stereo vision system, Procedia Eng. 69 (2014) 459–463, http://dx.doi.org/10.1016/j.proeng.2014.03.012.
[29] E. Todorov, Convex and analytically-invertible dynamics with contacts and constraints: Theory and implementation in mujoco, in: 2014 IEEE International Conference on Robotics and Automation, ICRA, IEEE, 2014, pp. 6054–6061, http://dx.doi.org/10.1109/ICRA.2014.6907751.
[30] Q. Chen, Y. Zhou, Y. Wang, M. Zhu, L. Guo, C. He, Research on stability and accuracy of the OptiTrack system based on mean error, in: S. Nakashima, S. Mu, H. Lu (Eds.), International Symposium on Artificial Intelligence and Robotics 2021, SPIE, 2021, p. 75, http://dx.doi.org/10.1117/12.2605796.
[31] G. Nagymáté, R.M. Kiss, Motion capture system validation with surveying techniques, Mater. Today Proc. 5 (13) (2018) 26501–26506, http://dx.doi.org/10.1016/j.matpr.2018.08.107.
[32] F. Vicentini, Collaborative robotics: A survey, J. Mech. Des. 143 (4) (2020) http://dx.doi.org/10.1115/1.4046238, 040802.

Leon Žlajpah received his DSc in Electrical Engineering from the University of Ljubljana, Ljubljana, Slovenia in 1989. He started working as a researcher at the Jožef Stefan Institute in 1981 and has been a senior consultant since 2009. From 2005 to 2014 he was Head of the Department of Automation, Biocybernetics. His main research interests include modeling and simulation of robotic systems and advanced control systems for robots. His contributions are in the areas of control of redundant robots, coherent robot control, sensor systems, robot applications and, more recently, control of robots in human interaction. He has been leader of several national research projects and bilateral applied projects with companies. He has received several awards for his research work in robotics and applications. Among them is a national award for research excellence in robotics.

Tadej Petrič is a senior research associate in the Department of Automation, Biocybernetics and Robotics at the Jožef Stefan Institute and an assistant professor at the Jožef Stefan International Postgraduate School, Slovenia. He is also the head of the Laboratory for the Advancement of Collaborative Robot Behavior in Physical Human–Robot Interaction (CoBoTaT). In 2015, he was a postdoctoral fellow at Biorob (Prof. Auke Ijspeert lab) at École polytechnique fédérale de Lausanne (EPFL). In 2013, he received a PhD in Robotics from the Faculty of Electrical Engineering, University of Ljubljana. He conducted part of his PhD research in the Department of Robotic Systems for Dynamic Control of Legged Humanoid Robots at the German Aerospace Center (DLR) in Germany. In 2013, he was a visiting researcher at ATR Computational Neuroscience Laboratories in Japan. His current research focuses on the design of biologically plausible robotic controllers that achieve robustness and adaptation to changing environments comparable to humans.